NRIAG JOURNAL OF ASTRONOMY AND GEOPHYSICS
2020, VOL. 9, NO. 1, 85–98
https://doi.org/10.1080/20909977.2020.1713583

Geoelectrical analysis for evaluating the aquifer hydraulic characteristics in Ain El-Soukhna area, West Gulf of Suez, Egypt

M. A. S. Youssef

Nuclear Materials Authority, Exploration Division, Cairo, Egypt

ABSTRACT

Ain El-Soukhna area is an important industrial area for building and construction, so we used the subsurface shallow geophysical method, as represented by geoelectric resistivity measurements (Vertical Electric Sounding (VES)). These are processed and interpreted in the forms of a geologic model composed of five geoelectric layers of varying resistivities, lithologies, depth-sand thicknesses. The thickness and true resistivity maps of the different layers and 2D geoelectric cross sections are generated for the represented layers to delineate their spatial distribution. The geoelectric Dar-Zarrouk parameters (Transverse Resistance and Longitudinal Conductance) were used to evaluate the electric anisotropy and aquifer hydraulic characteristics; such as hydraulic conductivity and transmissivity within the aquifer, as well as the groundwater quality (salinity of the aquifer) are estimated the true resistivity values acquired on the surface through the geoelectric resistivity survey.

ARTICLE HISTORY
Received 16 July 2019
Revised 11 November 2019
Accepted 4 January 2020

KEYWORDS
VES; electric resistivity; electric conductivity and Salinity

1. Introduction

Geoelectrical resistivity is a vital tool of the geophysical processes, which have candidate to be significant at a large scale, mostly for reconnaissance phase of the feasibility procedure (Dahlin et al. 1999; Albouy et al. 2001; Ismail 2003; Cavinato et al. 2006; Ganerød et al. 2006; Asfahani 2007; Al Temamy et al. 2008; Elwaseif et al. 2012; Abu El-Ata et al. 2016; Abou Heleika et al. 2018; Sharaf El Dein et al. 2019). They are applied (VESes) to investigate nature, types lithostratigraphy (Lithofacies), civil engineering, geoenvironmental investigations and geometry of a shallow and deep aquifers.

In addition to interpreting the data specifically, the knowledge of the geological setting of the area is significant. The ability of geoelectrical investigation is to refer to the changes in the subsurface layers conditions by means of varying resistivities candidate then to be significant tools for the pre-investigation and production procedures (Abu El-Ata and Ismail 1999; Abu El-Ata et al. 2016). However, it is not constantly potential to relate a resistivity variation to a specific rock condition or property. Evaluating the aquifer hydraulic characteristics is significant to solve several hydrogeological problems, while the transverse resistance, longitudinal conductance, electric anisotropy, hydraulic conductivity and transmissivity are playing a vital role in assessing the hydrogeological conditions.

The present study is objected to evaluate such aquifer hydraulic parameters, as the electric anisotropy, hydraulic conductivity and transmissivity of the studied section, using the secondary geoelectric Dar-Zarrouk parameters, as well as estimating the salinity from the acquired true resistivity values. Before performing the mentioned parameters, quantitative interpretation was carried out to determine the true resistivity and thickness of each layer, and represented them as 2D geoelectric cross-sections and areal distribution maps.

2. Geology of the area

Ain El-Soukhna area is a part of the Suez Governorate and sites at the western side of the Gulf of Suez, Egypt (Figure 1). Geomorphologically, the area under consideration is represented by a coastal plain bordered from the east by the Suez – Hurghada highway and the Gulf of Suez feature and from the south by El Galala El-Bahariya plateau. Further, a number of major wadis dissect the neighbourhood of the concerned area; among these: wadi Hagul at the north, wadi El Badaa at the central and Wadi Ghewibba to the south (Figure 2) (Conoco 1987). Moreover, the Cairo – Ain El Soukhna new road lies to the northwest of the area under investigation, mostly perpendicular to the Suez-Ain El Soukhna road along the Gulf of Suez coast.

Geologically, the exposed surface geology of the study area and its surroundings are formed from rock types ranging in age from Upper Cretaceous to Holocene (Figure 2). However, the Upper Cretaceous rocks are composed of limestone and dolomite (Galala Formation). It is located to the west central and southern parts of the study area; the Middle Eocene rocks are consisted of massive limestone and marl

CONTACT M. A. S. Youssef shokryam@yahoo.com Nuclear Materials Authority, Exploration Division, P.O. Box 530, Cairo, Egypt

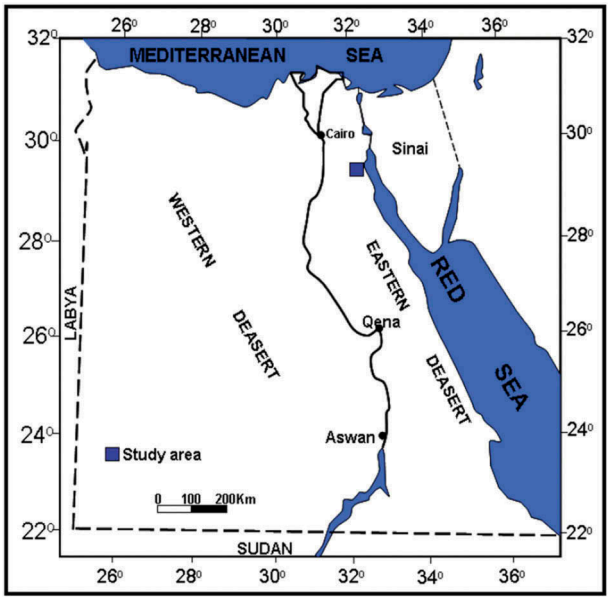

Figure 1. Location map of Ain El-Soukhna area, Egypt.

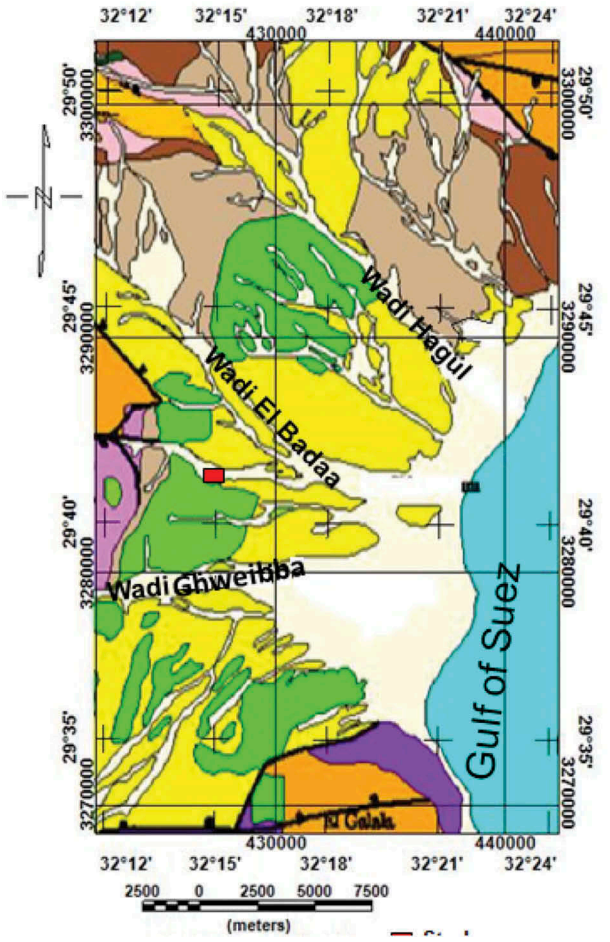

Figure 2. Surface geologic map for the vicinity of the studied area (Conoco; 1987).

(Mokattam Formation), which lies at the northeastern, northwestern, south central and west central parts of the study area; the Upper Eocene rocks are made up of bedded limestone and shale represented by Wadi Hof Formation, that appeared at the northern part of the study area; the Middle Miocene rocks are composed of limestone, shale and marl (Hommath Formation) which appears at the northern part of the study area; the Upper Miocene rocks are consisted of calcareous sandstone, marls and shales (Hagul Formation) which lies at the western part of the study area; and the Pleistocene sediments are made up of shales and sandstones and surrounded the study area, while the Holocene deposits are constituted from alluvium, sands and gravels, and cover mostly the surface geology of the study area, as shown in Figure 2.

Structurally, the area under investigation and the surrounding parts were dissected by many normal faults; the majority has NW-SE direction. The first normal faults are located west Wadi El Badaa. The second normal faults are located at Northeastern Wadi Hagul. There is a normal fault, which cuts the southern part of the study area parallel to Wadi Ghewibba and has the E-W trend, where the Middle Miocene layers formed this part of the El Galala El Baharyia plateau at high elevations, north of the fault in front of the faulted layers of the Middle Miocene, to the south of this normal fault. (Mohamed 2003).

3. Geoelectrical investigation

3.1. Geoelectrical measurements

The Vertical Electrical Sounding (VES) method is carried out in the mentioned study for the purpose of subdividing the shallow section into layers with varying lithologies and water contents in the subsurface of Ain El-Soukhna area, and also for determining the geoelectric Dar-Zarrouk parameters for evaluating the aquifer hydraulic characteristics. In the present study, 20 vertical electrical soundings (VESes), using Schlumberger array, are conducted to investigate the vertical distribution of the examined resistivity layers (Figure 3). The spacing between the VESes locations are controlled by the topographic and geologic conditions of the site. The maximum distance AB/2 of VESes is 600 m. The used resistivity metre is SYSCAL, of IRIS Instruments, French, with a microprocessor, digital display and RS-232C interface for PC data dump. SYSCAL-R2 has a transmitter and receiver in the same unit with high power signals. The apparent resistivity values measured by using Schlumberger arrangement were plotted on a log-log graph paper to obtain the field resistivity curves.

3.2. Geoelectrical analysis

Schlumberger configuration was applied on the injected current and the produced potential difference to calculate the apparent resistivity values (ρa), which are plotted versus AB/2 on a log-log graph paper to perform the field resistivity curves. One of the utilities of the log-

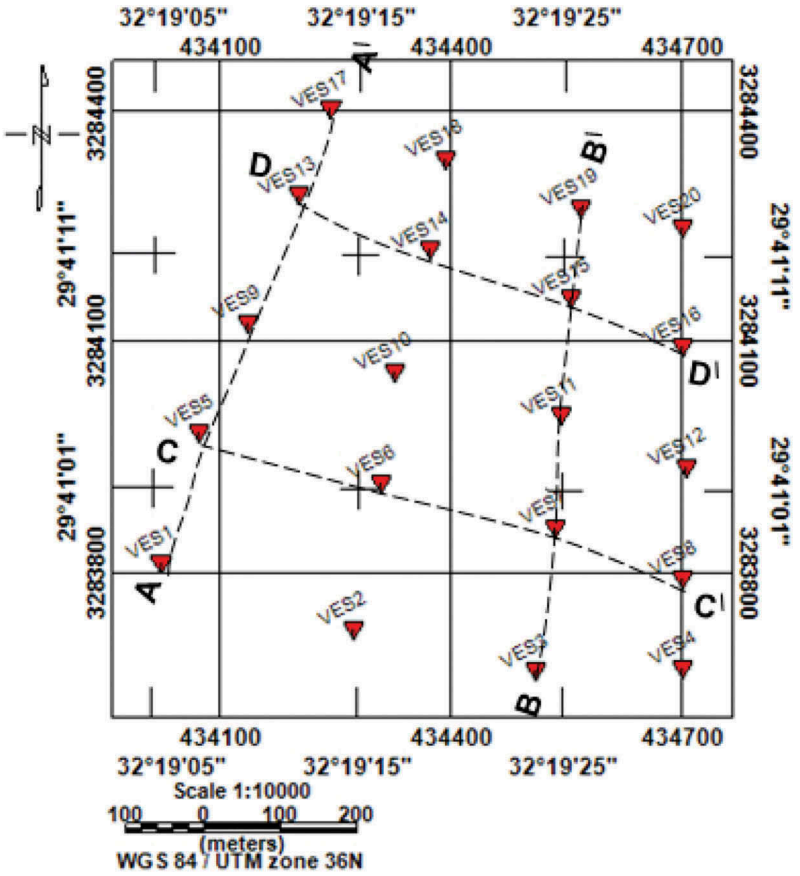

Figure 3. The VESes and 2D geoelectric cross-section locations along Ain El-Sokhna area. Electrode spacing (AB/2), or depth, in metre.

log plot confirms the near-surface resistivity differences and inhibits the differences at greater depths. This is significant, because the interpretation of the results depends mainly on the small differences in resistivity, which taking place at shallow depths. Due to the theoretical curves are generally smooth, the field curves should be smoothed, before carrying out their interpretation to neglect the obvious errors and effects of lateral variability. Isolated one-point spike in the resistivity is neglected instead of interpolated. The resistivity curves should be investigated for the apparent deformation, because of the effects of lateral differences.

Comparing with the theoretical multi-layer curves is helpful in detecting the layered geologic model. The field data were processed, using special software to force and reduce the different segments of the sounding curve into a continuous curve to remove the noises from the curve and to plot the corrected sounding curve. So, the data analysis was carried out by using two appropriate geoelectric softwares, which allow the analyst to achieve the equivalent true resistivity (ρ) model for each sounding. Subsequently, the data were interpreted quantitatively via the Ato program of Zohdy and Bisdorf (1989) to achieve the multi-layer model, and the Resist of Velpen (1988) to perform the layering model, where the automatic curve appropriate computer program results in a geoelectric model, the calculated apparent resistivity of which meets the given field curve roughly exactly (Figure 4), in addition to the regional background on the geology of the area are used to construct a preliminary model, that would fairly fit the observed field curves. This is after a minimum number of non-automatic iterations, which in turns represent the input model for Resist program.

Zohdy and Bisdorf (1989) process is adjusted to change the values of (AB/2) and (ρa) into a multi-layer model. It is an entirely automated and fast refined method, depended on obtaining the interpreted depths and true formation resistivities from the shifted electrode spacings and the modified apparent resistivities. Based on Sadek et al. (1987), an additional information about the subsurface variations within any selected geoelectric layer can be provided via constructing the n-layer model by Ato program (Zohdy and Bisdorf 1989) (Figure 4(a)). This is after a minimum number of non-automatic iterations, which contribute to perform the input model of the Resist of Velpen (1988), (Figure 4(b)). This program was generated for 1D automated and interactive semi-automated interpretation of vertical electrical sounding.

3.3. Geoelectrical discussion and results

A. Spatial distribution of the model parameters

The spatial distribution of the model involves the lateral and vertical variations of the true resistivities and

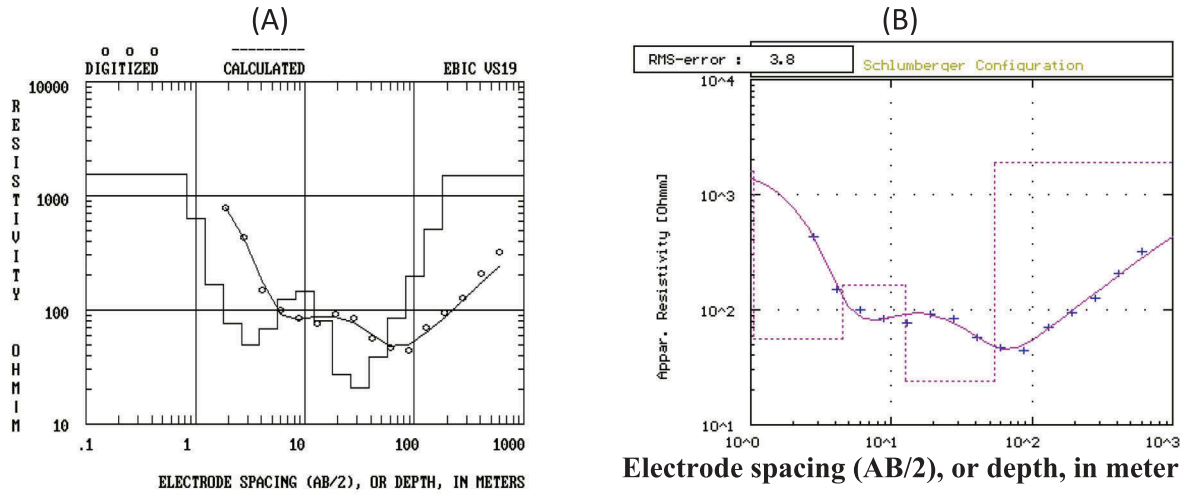

NO.	Interpreted Geology	Resistivity (Ω.m)	Thickness (m)	Depth (m)
1	Dry sands and gravels	1571	1	1
2	Saturated sands and gravels	55.5	3.4	4.4
3	Marly sandstone	162	8.2	12.6
4	Sandy shale	24	42	54.6
5	Massive limestone	1912	-----	------

Figure 4. Interpreted layering curve of VES 19, an example, by (A) .Zohdy and Bisdorf (1989) and (B) Resist, Velpen (1988).

thicknesses through the study area. To represent the areal distribution of the resulting data, two coloured images are generated for each resistivity layer; resistivity coloured image and thickness coloured image.

3.3.1. Areal distribution maps of the model parameters

3.3.1.1. Dry sands and gravels. Figure 5(a) and 5(b) show the resistivity and thickness coloured images, with the localities of the first layer (dry sand and gravels), which has a range of true resistivities reach to (42–6070 Ohm.m) and a maximum thickness about 4.8 m. The resistivities of this layer reach their highest values at the north western, southwestern and north-eastern parts of the area, which might be classified as coarse dry sands. Some of the external parts are characterised by moderate resistivity values (less than 900 Ohm.m), which may be described as fine dry sands. The thickness coloured image map of the first layer (Figure 5(b)) shows that, the minimum thickness (less than 1 m) is recorded at the western and southeastern parts of the study area.

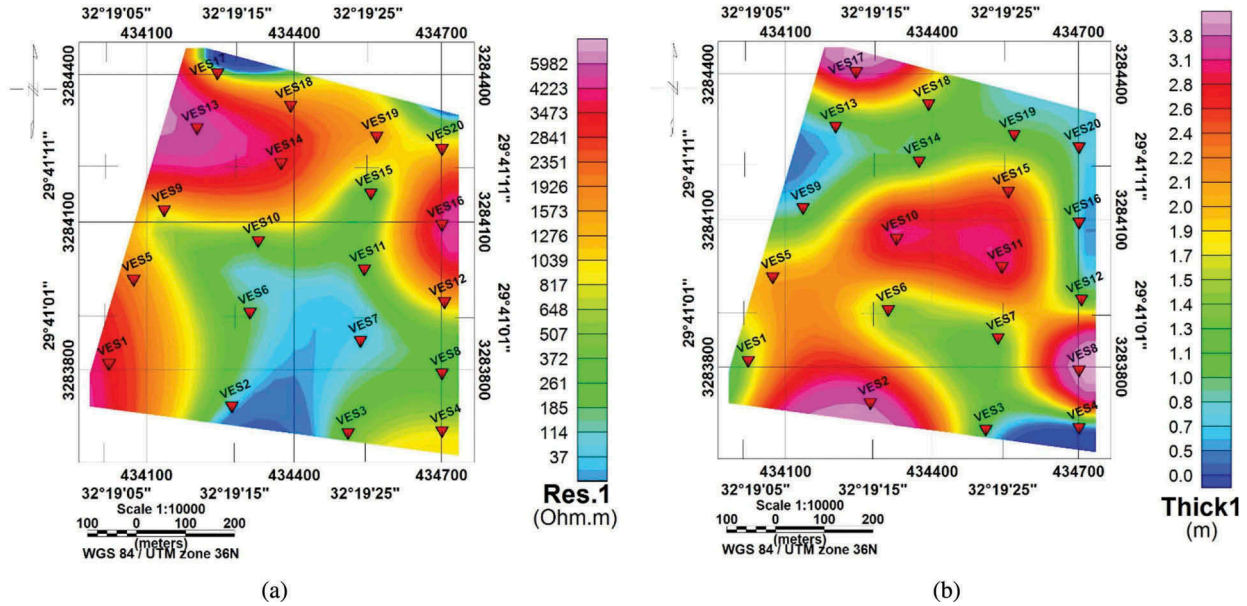

(a) (b)

Figure 5. (a) True resistivity coloured image of dry sands and gravels. (b) Thickness coloured image of dry sands and gravels.

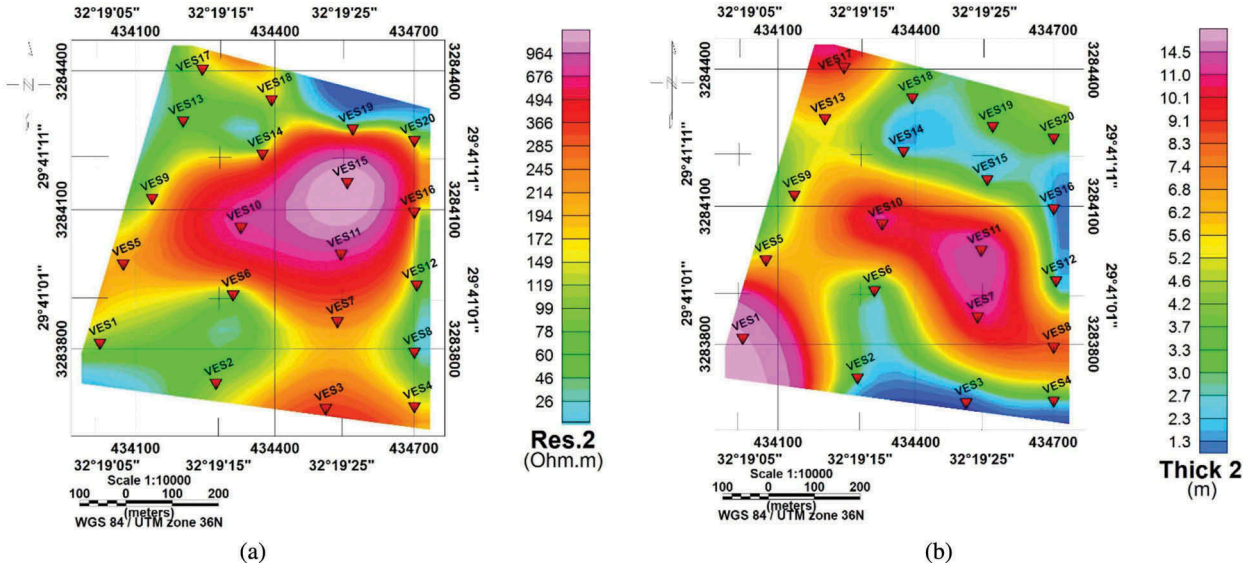

(a) (b)

Figure 6. (a) True resistivity coloured image of saturated sands and gravels. (b) Thickness coloured image of saturated sands and gravels.

3.3.1.2. Sands and gravels saturated with fresh-water. Figure 6(b) exhibits the resistivity coloured image and the localities of the saturated sands and gravels layer, the highly resistive zones (more than 300 Ohm.m) are noticed at the north central and southeastern parts of the study area. The western part has moderate to low resistivity values ($50 > \rho < 300$ Ohm.m), which decrease to less than 50 Ohm.m at some parts of the northeastern part of the study area.

This layer is found to be thicker of more than 27 m (Figure 6(b)) at the southwestern part of the study area. On the other hand, the thickness decreases to be less than 3 m at the northeastern and southeastern parts of the study area. The larger thickness of this layer is associated with lower resistive sediments of sands and gravels saturated with fresh water.

3.3.1.3. Marly sandstone. Figures 7(a) and 7(b) show the resistivity and thickness coloured images with the localities of the third layer (calcareous marl sandstone), which has a range of true resistivities reach to (88–1700 Ohm.m) and a maximum thickness of about 48 m at VES 8. The resistivities of this layer reach their highest values at the northwestern, southwestern, north central and southeastern parts of the area, which might be classified as highly compacted sandstone. Some of the external parts at the northeastern and northwestern sites are characterised by low resistivity values (less than 300 Ohm.m), which may be described as marly sandstone. The thickness coloured image map of the third geoelectric layer (Figure 7(b)) shows that, the minimum thickness (less than 5 m) is recorded at the northern and southeastern parts of the study area.

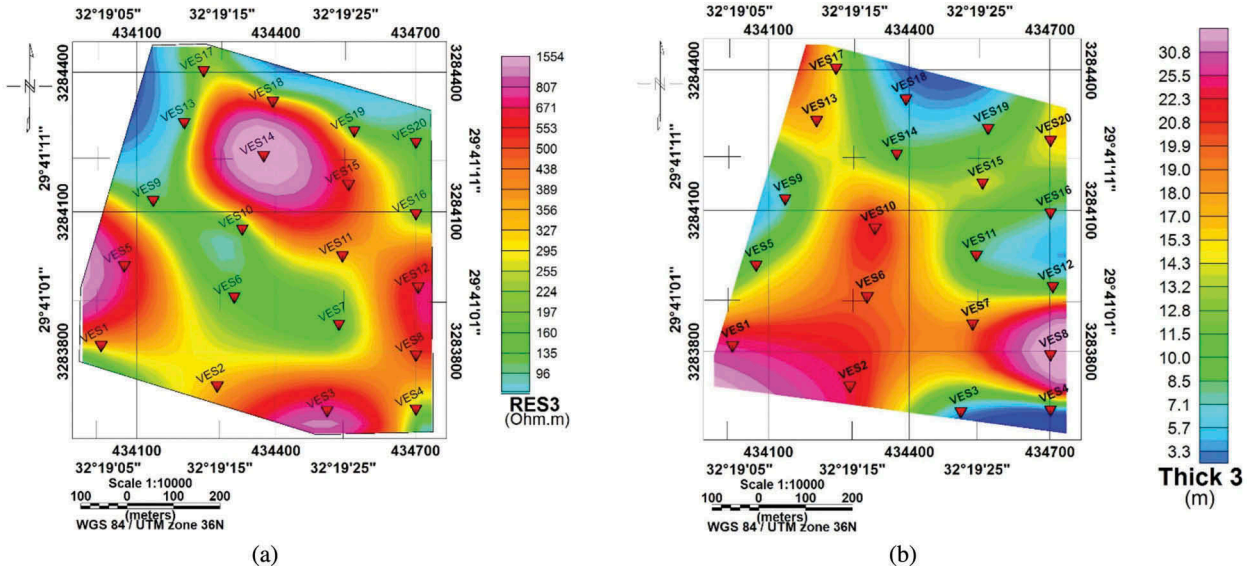

(a) (b)

Figure 7. (a) True resistivity coloured image of marly sandstone. (b) Thickness coloured image of marly sandstone.

3.3.1.4. Sandy shale saturated with salty water. Figure 8(a) reveals the true resistivity coloured image and the localities of the sandstone and shale saturated with salty water layer. The south central and central parts possess the lowest resistivity values (less than 10 Ohm.m) which meaning the abundance of saline water intrusion within aquifer. The resistivity values (more than 25 Ohm.m) are recorded at the western and southeastern parts of the area, reflecting the decreasing of saline water intrusion within aquifer. Thickness coloured image of this layer (Figure 8(b)) shows that, the lowest thickness values are less than 60 m and noticed at the northwestern, east central and southern parts of the area. Meanwhile, the highest thickness values are more than 170 m that recorded at VESes 5, 10 and 11, especially at the central part of the area. The values of computed electric resistivity, thickness and depth to the top of this layer are listed in Table 1 for each VESes.

3.3.1.5. Massive limestone. Figure 9 exhibits the resistivity coloured image and the localities of the massive limestone layer, the highly resistive zones (more than 2000 Ohm.m) are noticed at the northwestern, southwestern and southeastern parts of the study area. The other parts of the south central and north central parts have moderate to low resistivity values (values range between less than 2000 Ohm.m and more than 500 Ohm.m), which decrease to less than 500 Ohm.m at some parts of the west central and northeastern parts of the study area.

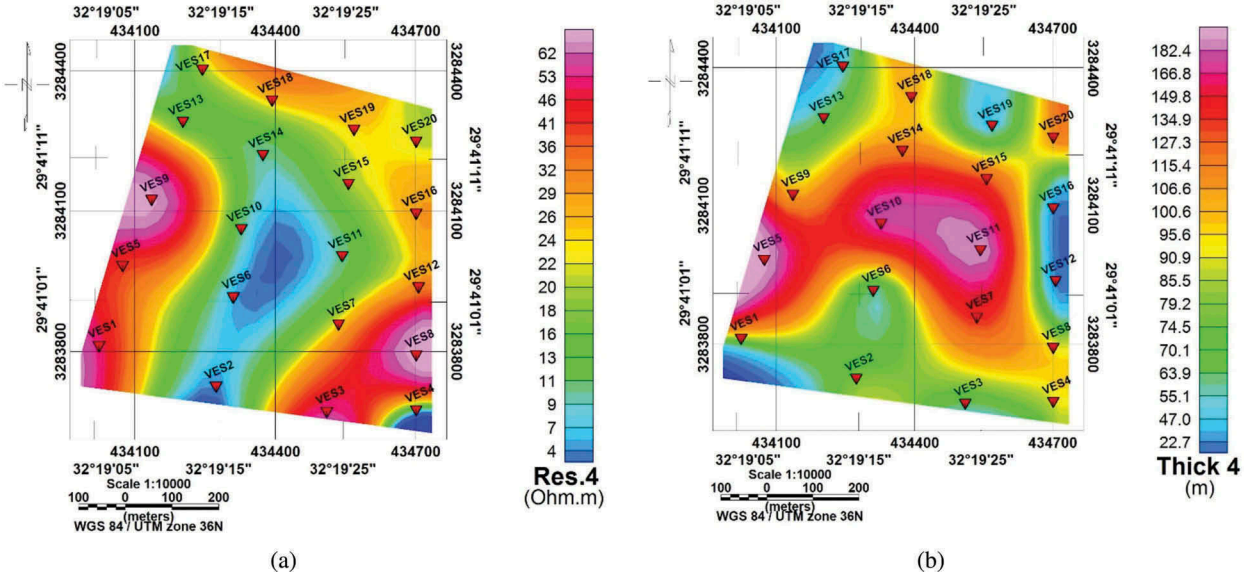

Figure 8. (a) True resistivity coloured image of sandy shale saturated with water. (b) Thickness coloured image of sandy shale saturated with water.

Table 1. Summary of results of aquifer properties of VES points.

VES point	Depth to water(m)	Layer resistivity (Ωm)	Electric conductivity EC (dS/m)	Aquifer thickness (m)	Transverse Resistance (R) ρb (ohm.m^2)	Anisotropy (dimensionless)	Hydraulic conductivity (m/day)	Transmissivity (m2/day)	Groundwater yielding capacity/salinity hazard	Salinity (ppm)
VES1	55.6	57.0	0.18	64.0	3648	0.017	0.640	40.71	Moderate/low	112
VES2	29.0	4.1	2.44	78.0	319.8	0.743	0.620	48.71	Moderate/high	1561
VES3	8.4	51.0	0.2	68.0	3468	0.015	0.630	43.03	Moderate/low	125
VES4	12.5	15.0	0.67	93.7	1405.5	0.040	0.610	57.34	Moderate/low	427
VES5	20.2	37.5	0.27	209.0	7837.5	0.171	0.530	110.09	High/low	171
VES6	23.5	5.0	2	53.0	265	0.063	0.650	34.19	Moderate/high	1280
VES7	31.0	23.0	0.43	140.0	3220	0.219	0.580	80.67	Moderate/low	278
VES8	61.6	84.0	0.12	96.9	8139.6	0.171	0.610	59.05	Moderate/low	76
VES9	12.0	77.0	0.13	97.0	7469	2.671	0.610	59.10	Moderate/low	83
VES10	38.0	9.0	1.11	187.0	1683	0.496	0.540	101.36	High/medium	711
VES11	24.0	10.0	1	199.0	1990	0.680	0.530	106.20	high/medium	640
VES12	9.4	26.0	0.38	15.8	410.8	0.017	0.680	10.70	Moderate/low	246
VES13	23.8	12.0	0.83	63.5	762	0.024	0.640	40.41	Moderate/medium	533
VES14	11.3	8.0	1.25	111.0	888	0.041	0.600	66.41	Moderate/medium	800
VES15	19.0	20.0	0.5	128.0	2560	0.085	0.590	74.91	Moderate/low	320
VES16	11.1	30.0	0.33	22.0	660	0.004	0.670	14.78	Moderate/low	213
VES17	26.5	18.9	0.53	51.8	979.02	0.017	0.650	33.47	Moderate/low	339
VES18	8.7	26.5	0.38	106.6	2824.9	0.091	0.600	64.15	Moderate/low	242
VES19	12.7	24.0	0.42	42.0	1008	0.025	0.650	27.49	Moderate/low	267
VES20	19.8	21.0	0.48	117.0	2457	0.120	0.590	69.46	Moderate/low	305

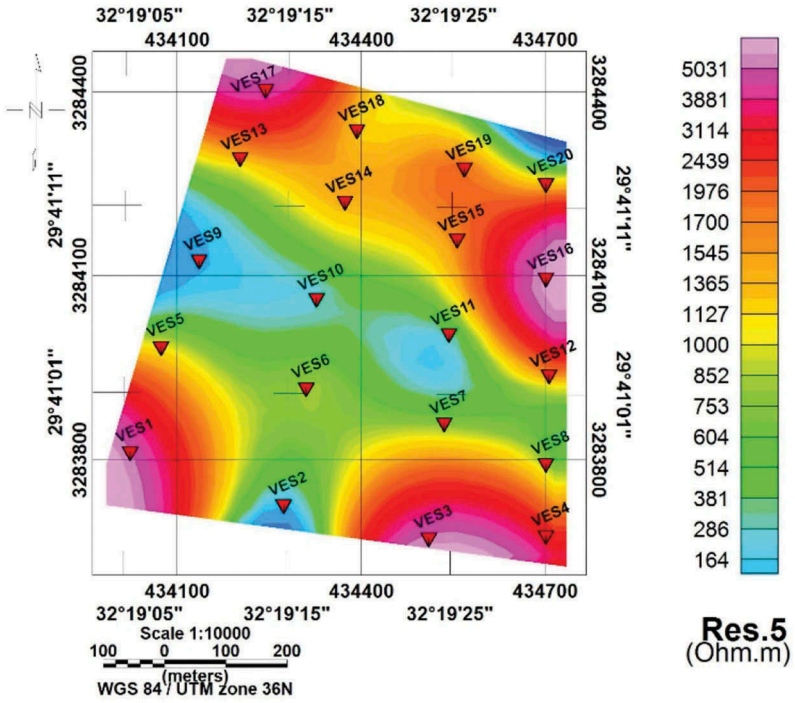

Figure 9. True resistivity coloured image of massive limestone.

3.3.2. Vertical distribution of the model parameters

The established resistivity modelling contributes for constructing four 2-D reliable geoelectric cross-sections, which show three geoelectric layers (Figure. 10(a–d)). It is worth-mentioning that, the first geoelectric layer (fine to moderate dry sand) is thin and of high resistivity. So, it is not recognisable in some parts of the 2D geoelectric cross-section, causing mis-interpretation for the first layer (fine to moderate dry sand); the second (sands and gravels saturated with fresh water); the third geoelectric layer is calcareous marl sandstone; the fourth geoelectric layer is sandstone and shale saturated with water and the last geoelectric layer is represented by massive limestone. Therefore, the four generated geoelectric sections are built and discussed in view of their directions, lengths and included soundings.

3.3.2.1. Geoelectric cross-section A-A`. This section (Figure10(a)) extends for about 0.65 km and passes through VESes 1, 5, 9,13 and 17, respectively, across the western part, from the south to the north directions of the area. The resistivity values of the aquifer

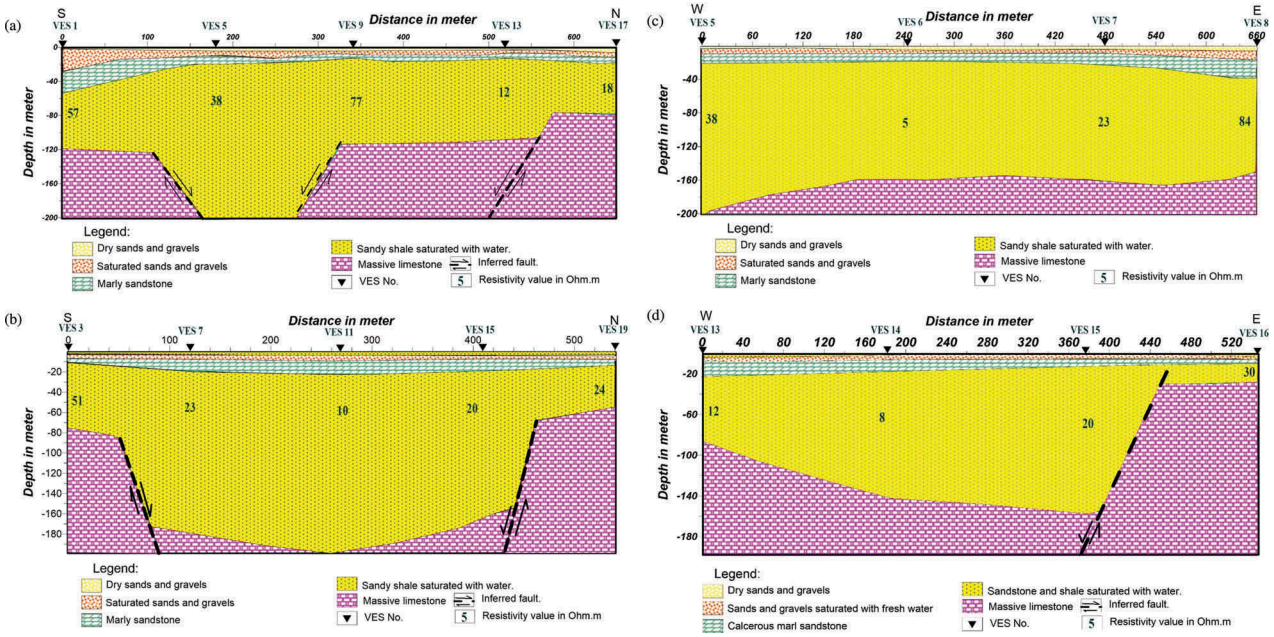

Figure 10. (a) Geoelectric cross section A-A`of the VESes 1, 5, 9,13 and 17. (b) Geoelectric cross-section B-B`of the VESes 3, 7, 11, 15 and 19. (c) Geoelectric cross-section C-C`of the VESes 5, 6, 7 and 8. (d) Geoelectric cross-section D-D`of the VESes 13, 14, 15 and 16.

increase relatively towards the southern and central parts of this section (towards VESes 1 and 9), as compared with the values recorded at the rest of the section for the same layer. In this section, there are three normal fault trending E-W, which tend to increase the thickness of aquifer for more than 170 metres

3.3.2.2. Geoelectric cross-section B-B`. The second section (Figure 10(b)) is approximately parallel to the first one and extends also from the South to the North directions. It passes through VESes 3, 7, 11, 15 and 19, respectively. The sandstone and shale saturated with water recorded the lowest resistivity value of 10 Ohm.m at VES 11. The thickness of this layer increase, towards the central part of this section, which result from two normal faults formed a grabben at the central part of this section.

3.3.2.3. Geoelectric cross-section C – C`. This geoelectric section extends for about 0.66 km, from the West to the East directions. It is represented by VES stations 5, 6, 7 and 8, respectively (Figure 10(c)). The VESes 5, 6, 7 and 8 recorded a noticeable extension of the fourth geoelectric layer along the whole section from the western to the eastern directions, for average thickness of 160 m. Also, the resistivity values decrease towards the central part of the section due to the sea water intrusion.

*3.3.2.4. Geoelectric cross-section D-D`.* This section (Figure 10(d)) passes through VESes 13, 14, 15 and 16, respectively. It extends from the western to the eastern directions and approximately perpendicular to the sections A – A` and B – B`and parallel to the geoelectric section C – C` at the south-central part. The sandstone and shale are saturated with water recorded the lowest resistivity value at the western part of this section, with thin thickness through VES16, due to the presence of deeper inferred normal fault between VES15 and VES16.

4. Aquifer hydraulic parameters

The geoelectric resistivity method is primarily used to measure the potential differences on the surface caused by the current flow within the ground. However, the mechanism judging the electric current, conductance and fluid flow are mainly controlled by the same physical parameters and lithological conditions. Therefore, the hydraulic and electric conductivities are generally dependent upon each other. These parameters are depended on the consideration of a column of unit square cross-sectional area (m^2) cut out of layers group of infinite lateral extent (Khalil 2009).

4.1. Secondary geoelectric (Dar-Zarrouk) parameters

The fundamental parameters, that describe the geoelectric layer have been derived from the qualitative analysis of the electrical sounding, as the resistivity (ρi) and thickness (hi) values along the study area; where the subscript "i" refers to the layer position in the geoelectric section. Some geoelectric parameters can be derived from these basic parameters, such as the total longitudinal conductance (S) and total transverse resistance (T). These have been illustrated by Maillet (1947), as the Dar-Zarrouk parameters, which are mathematically derived as apparent parameters:

4.1.1. Total longitudinal conductance

$$S = h1/\rho1 + h2/\rho2 + h3/\rho3 + \ldots\ldots + hn/\rho n\left(\Omega^{-1}\right) \quad (1)$$

4.1.2. Total transverse resistance

$$T = h1 * \rho1 + h2 * \rho2 + h3 * \rho3 + \ldots\ldots + hn * \rho n\left(\Omega m^2\right) \quad (2)$$

where: i = 1, 2, 3 … n^{th} layer.

While, the S and T have been defined as the Dar-Zarrouk parameters for individual layers or as a summation for a multi-layers (Maillet 1947).

The above-mentioned secondary parameters are derived for all the vertical electrical soundings data, using the results of the resistivity modelling of the VESes and represented in the form of areal distribution maps to describe those parameters.

Figure 11 illustrates the areal distribution map of the calculated Total Longitudinal Conductance (S) throughout the study area. Here also, a homogenous distribution in the S values could be observed. The lowest values increase in the S could be noticed at the north central and western parts. In addition to the middle part of the eastern side based on Oteri (1981) the decrease in the longitudinal conductance may correspond to the decrease in sea water intrusion. Therefore, the increase in the longitudinal conductance could be interpreted as a decrease in the transmissivity.

Figure 12 shows the areal distribution map of the calculated Total Transverse Resistance (T) throughout Ain El-Soukhna area. Homogeneity in the total transverse resistance could be noticed throughout the study area, except at the northeastern, northwestern and southwestern parts where an anomalous increase in the (T) could be observed. Based on Niwas and Singhal (1981), there is a direct relationship between the transmissivity and transverse resistance. They assumed that, the chemical quality of the groundwater within the evaluated zone remains relatively uniform. So, the present map of T shows a homogenous distribution in the electrical

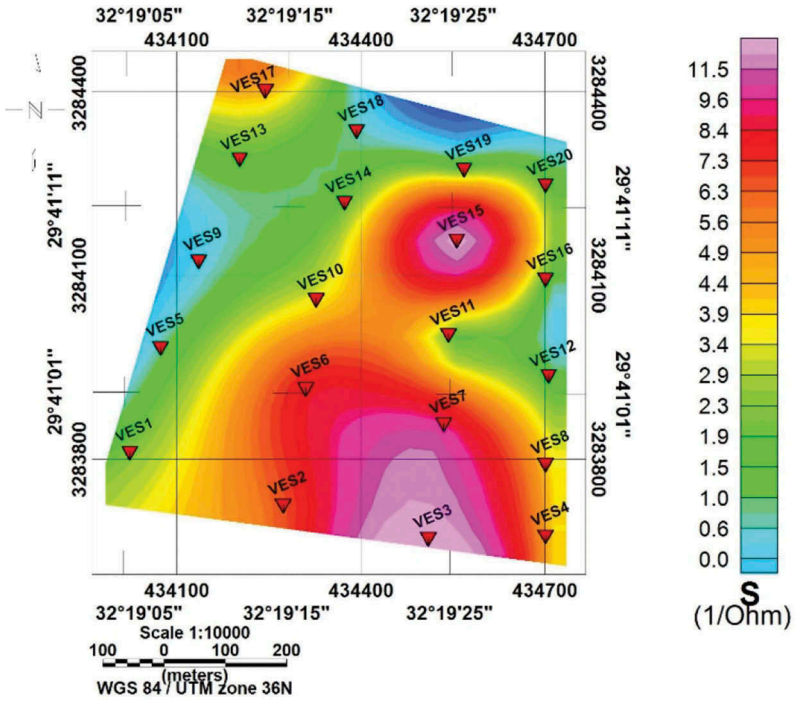

Figure 11. Total longitudinal conductance map of the study area.

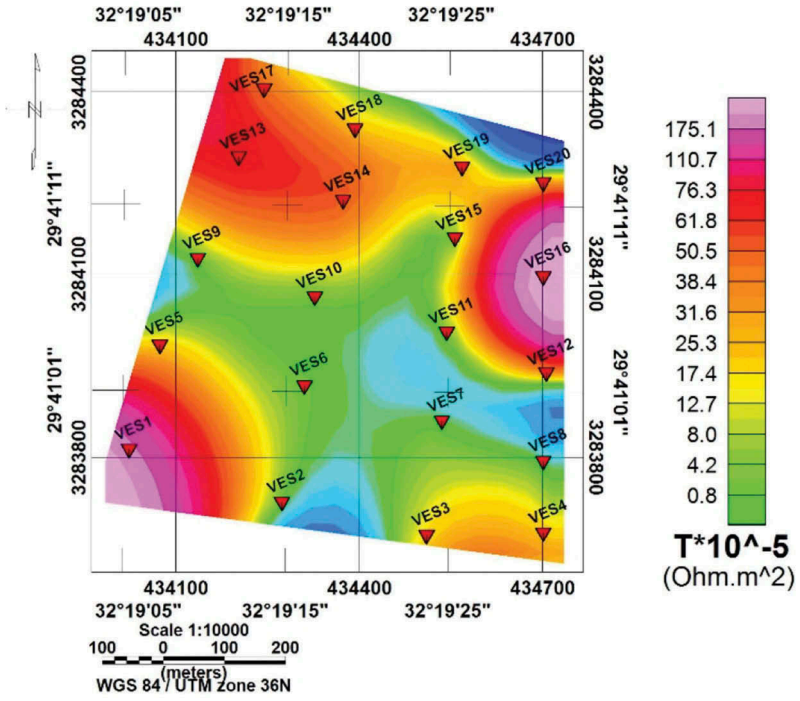

Figure 12. Total transverse resistance map of the study area.

transmissivity throughout the study area, except at the above-mentioned parts.

4.2. Electric anisotropy (l)

4.2.1. Average longitudinal resistivity

$$\rho L = H/S = S\ hi/(S\ hi/\rho i)\ (\Omega m) \tag{3}$$

where: H = h1+ h2+ h3+ … hn (Ωm)

4.2.2. Average transverse resistivity

$$\rho t = T/H = (S\ hi * \rho i)/Shi(\Omega m) \tag{4}$$

$$l = (\rho L/\rho t)^{\wedge 1/2} = (T * S/H)^{\wedge 1/2} \tag{5}$$

It is a dimensionless entity and Root Mean Square Resistivity. Figure 13 reflects the areal distribution of the electric anisotropy throughout the study area. The electric anisotropy calculated for the alteration of

electric resistivity in both the horizontal and vertical directions. It is well to know that, the variation of the isotropic layers (where anisotropic = 1.0) could be converted into an equivalent heterogeneous and anisotropic structure. Flathe (1955) interpreted this anisotropy as a result of alternating layers of shale and fine sands. The central, west central and south-central parts of the study area reflect an increase in the electric anisotropy, due to the presence of alternating increasing sea water intrusion and change in the rock types vertically and horizontally. Values of the computed electric anisotropy is listed in Table 1 for each VESes.

4.3. Electric hydraulic conductivity (K)

Due to the lack of hydraulic conductivity values from boreholes in the study area, the estimated hydraulic conductivity is assumed from Singh's equation (2005) to be relatively equal to the resistivity values of the aquifer through alternating layers of sand and shale saturated with saline water.

(Singh 2005) postulated an empirical relation to calculate the hydraulic conductivity in a fractured hard rock aquifer, as shown:

$$K = 8x10^{-6}e^{-0.0013\rho} \quad (6)$$

where: ρ is resistivity of the aquifer.

Figure 14 shows a range of hydraulic conductivity values, from 0.53 m/day to 0.68 m/day. It is noticed that, the northwestern and eastern parts have higher hydraulic conductivities. Meanwhile, the lowest values are recorded at the central and southwestern parts of the study area. Values of the computed electric hydraulic conductivity are listed in Table 1 for each VES.

4.4. Electric transmissivity (ET)

Henriet, 1976 described the aquifer transmissivity (the product of aquifer thickness and hydraulic conductivity) for all the sounding locations in the study area, including those parts due to there are no boreholes in the investigated area. The transmissivity computed from the relation below:

$$T = K * h \quad (7)$$

where T is the transmissivity in m^2/day and h is the aquifer thickness in metre

Transmissivity across the study area varies between 10 m^2/day and 110 m^2/day. Figure 15 shows the aerial distribution of the transmissivity obtained for the study area, showing parts of high and low transmissivities. It is noticed that, the transmissivities could be interpreted as decreasing with increasing the geoelectric Dar-Zarrouk parameters (Transverse Resistance, Longitudinal Conductance and the electric anisotropy), and them with increasing in sea water intrusion. Therefore, the productive potential of the aquifer indicates that, this location has the moderately potential for production, due to its moderate hydraulic conductivities and transmissivities. Values of the computed electric transmissivity of the saline aquifer is listed in Table 1 for each VES. Table 2 shows the classification of transmissivity magnitudes (Gheorghe 1978 and Krasny 1993).

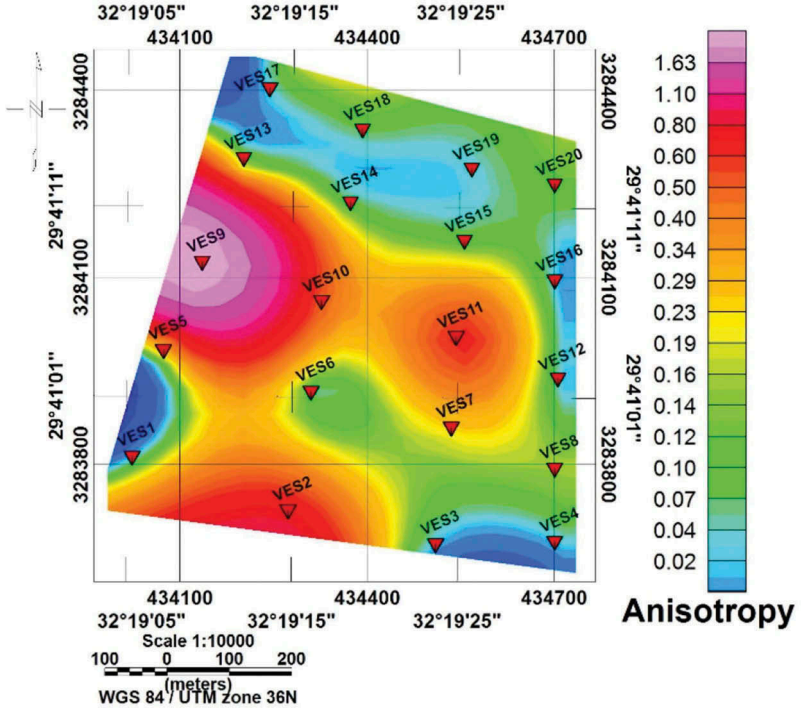

Figure 13. Electrical anisotropy map of the study area.

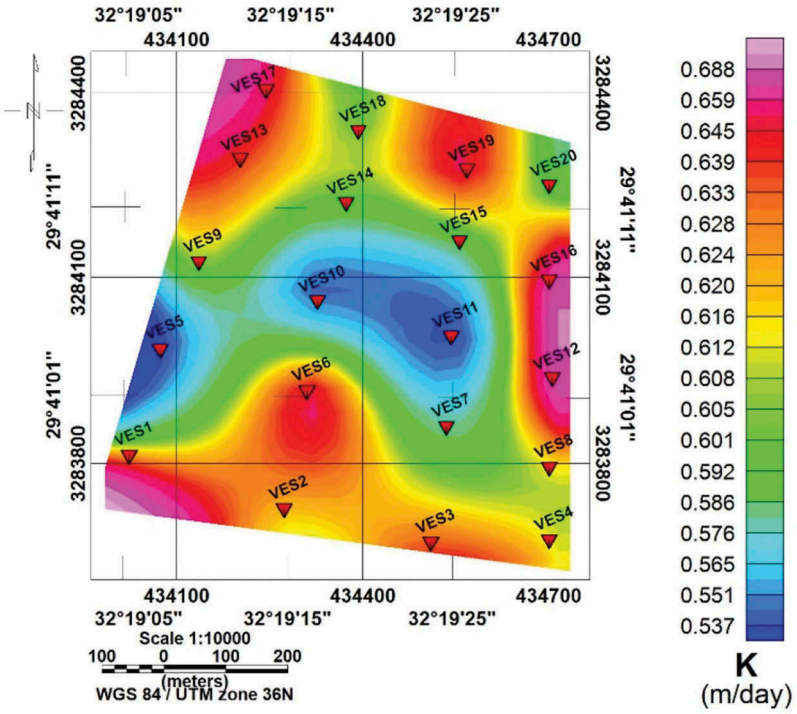

Figure 14. Hydraulic conductivity map of the study area.

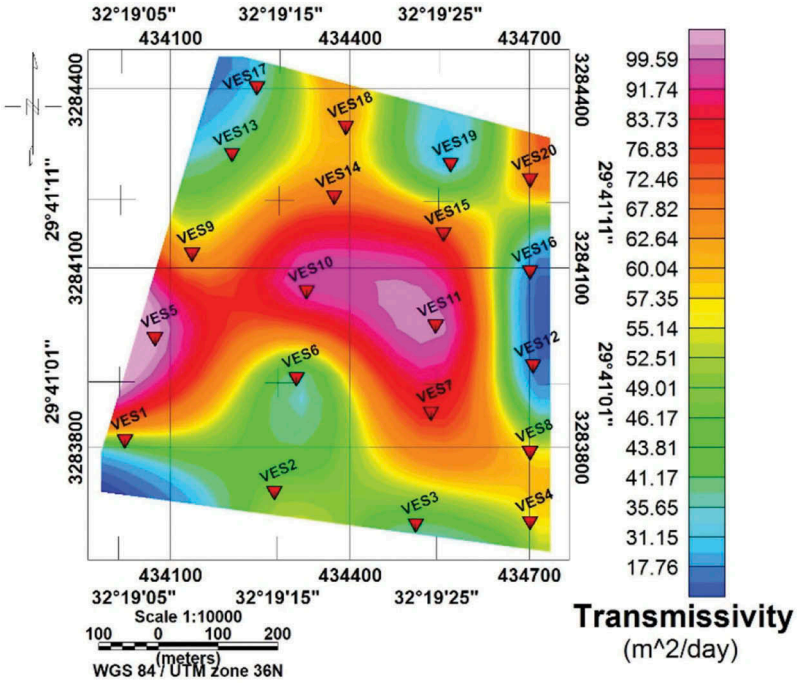

Figure 15. Transmissivity map of the study area.

4.5. Salinity

To detect the expected salinity, there is a function of its measured electrical conductivity, according to the relation:

$$\rho w = 1/EC \tag{8}$$

where: ρw is the electrical resistivity of groundwater (Ωm), EC is the electrical conductivity of groundwater (siemens/m(S/m) = 10*desi-siemens/m(dS/m)).

In this study, the groundwater resistivity (ρw) have been estimated from the geoelectric resistivity measurements via assuming that, the least resistivity value (high saturation zone) is relatively equal to the groundwater resistivity, and according to Hem (1970) and Iyasele et al. (2015), the relation between the electrical conductivity and total dissolved solids is (TDS):

$$TDS(\text{ppm or mg/l}) = 640 * EC(dS/m) \tag{9}$$

Table 2. Classification of the transmissivity magnitude (Gheorghe 1978 and Krasny, 1993).

	T (m^2/day)	Aquifer potential	Groundwater yielding capacity
1	**>1000**	Very High	Very high Withdrawal of great regional importance
2	100 – 1000	High	Withdrawal of lesser regional importance
3	**10 – 100**	Moderate	Withdrawal of local water supply (eg. small community)
4	**1 – 10**	Very low	Smaller withdrawal for local water supply (private consumption)
5	**0.1 – 1**	low	Withdrawal of local water supply with limited consumption
6	**< 0.1**	Negligible	Impermeable sources for local water supply are difficult

Figure 16 shows the areal distribution map of the salinity (water quality) throughout the study area. The rough estimation for groundwater salinity ranges of less than 1000 ppm in all VESes, except VESes 2 and 6. The lowest value of salinity recorded (less than 200 ppm) of VESes 1, 3,5, 8 and 9 at the eastern and western parts of the study area. Values of the computed salinity aquifer and evaluated salinity hazard class, according to the EC and TDS (Carrow and Duncan 1998; Iyasele et al. 2015) are listed in Table 3 for each VES. So, the aquifer is characterised by fresh, marginal to slightly brackish water.

5. Summary and conclusions

This work discusses the qualitative and quantitative interpretations of the surface geoelectric data of Ain El-Soukhna area, West Gulf of Suez, Egypt. The final resistivity model is consisted of five geoelectric resistivity layers distributed to be appropriate to represent the subsurface geologic layering of the study area. Lithologies, resistivities, depths and thicknesses of these layers are: surficial dry sand and gravels; sand gravels saturated with freshwater; marly sandstone, sandstone and sandy shale saturated with salty water and massive limestone. The areal distribution of the resistivity and thickness maps and 2D geoelectric cross-section are illustrated in the form of spatial distribution, either vertical or horizontal for each layer. The thickness aquifer increases at central parts, under

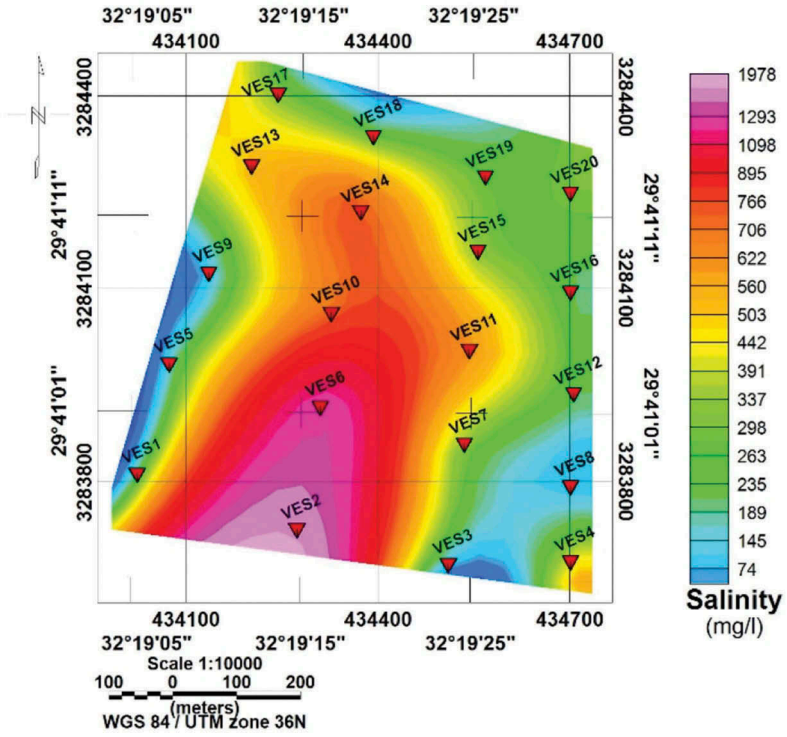

Figure 16. Salinity map of the study area.

Table 3. Total salinity hazard classification guidelines for the variable quality irrigation water, based on the EC and TDS (Carrow and Duncan 1998; Mayer et al. 2005).

Salinity Hazard Class	EC (dS/m)	TDS (ppm)	Description and use	Management Requirements
Low (Fresh)	<0.75	<500	Drinking and all irrigation	No detrimental effects expected.
Medium (Marginal)	0.75–1.5	500 – 1,000	Most irrigation, adverse effects on ecosystems become apparent	Moderate leaching to prevent salt accumulation.
High (Brackish)	1.5–3.0	1,000–2,000	Irrigation certain crops only; useful for most stock	Turf species/cultivar selection, good irrigation, leaching, drainage.
Very high (Saline)	>3.00	> 2,000	Useful for most livestock	Most salt-tolerant cultivars, excellent drainage, frequent leaching, intensive management.

VESes 5,7, 10, 14 and 18 of study area due to series of inferred normal faults and formed grabben structure.

Through the application of the geoelectric Dar-Zarrouk parameters, the study area shows the heterogeneous distribution in the TTR, TLC and l. The highest electric anisotropy values appear at the central, west central and south-central parts of the study area which reflect increasing sea water intrusion and variation in the rock types vertically and horizontally. The evaluation of the hydraulic conductivity and the transmissivity for the vertical electrical soundings locations along the study area. The lowest hydraulic conductivity (less than 0.56 m^2/day) and the highest transmissivity value (more than 100 m^2/day) were obtained at the VESes No 5, 10 and 11 to be withdrawal of lesser regional importance of groundwater potentiality. According to the computed salinity, the highest salinity within the aquifer tends to be at the southern part of the study area, which recorded maximum salinities of 1561 and 1280 under VESes 2 and 6, respectively. The aquifer is thus characterised by fresh water, except VESes 2 and 6 having sea water intrusion supported.

Acknowledgements

I would like to thank Prof. Ahmed S. A. Abo El-Ata and Prof. Adly Abdel Aziz for suggesting a number of improvements in this manuscript. I also would like to extend my thanks to Prof. NIRAG's reviewers for reviewing of my paper.

Disclosure statement

No potential conflict of interest was reported by the author.

ORCID

M. A. S. Youssef http://orcid.org/0000-0002-1553-2021

References

Abou Heleika M, Ismail E, Ahmed M. 2018. Delineation of contamination zone using geophysical and hydrogeochemical methods around the El Moheet drain in the El Minia district, Upper Egypt. Arabian J Geosci. 11:625. doi:10.1007/s12517-018-3927-2

Abu El-Ata AS, Yousif MS, Youssef MAS, Elkotb AS. 2016. Geoelectrical analysis for evaluating the aquifer hydraulic characteristics of Darb El Arbein area, South Western Desert, Egypt, Egy. J Appl Geophys. 15(2):91–106. Sept 2016.

Abu El-Ata ASA, Ismail ISA. 1999. The role of geoelectric interpretation in delineating the saline water intrusion of the Gulf of Suez along the western coast of Sinai Peninsula, Egypt. GAW 4. Int on Geol.of The Arab World Cairo Univ. 1:1047–1068.

Al Temamy AMM, Khaled MA, Barseem MSM. 2008. Use of geoelectrical techniques to determine the impact of facies changes on groundwater potentials and water logging in the area south of lake manzala, east nile delta, Egypt. Egypt J Desert Res. 58(2):1–18.

Albouy Y, Andrieux P, Rakotondrasoa G, Ritz M, Descloitres M, Join J, Rasolomanana E. 2001. Mapping coastal aquifers by joint inversion of DC and TEM soundings: three case histories. Groundwater. 39:87–97.

Asfahani J. 2007. Geoelectrical investigation for characterizing the hydrogeological conditions in semi-arid region in Khanasser valley, Syria. J Arid Environ. 68:31–52.

Carrow RN, Duncan RR. 1998. Salt-affected turfgrass sites: assessment and management. Chelsea (MI): Ann Arbor Press. p. 185.

Cavinato GP, Di Luzio E, Moscatelli M, Vallone R, Averardi M, Valente A, Papale S. 2006. The new Col di Tenda tunnel between Italy and France: integrated geological investigations and geophysical prospections for preliminary studies on the Italian side. Eng Geol. 88 (2):90–109.

Conoco. 1987. Geological map of egypt. scale 1:500,000, NH36 SW-BENI SUEF sheet.

Dahlin T, Bjelm L, Svensson C. 1999. Use of electrical imaging in site investigations for a railway tunnel through the Hallandsås Horst, Sweden. Q J Eng Geol. 32:163–172.

Elwaseif M, Ismail A, Abdalla M, Abdel-Rahman M, Hafez MA. 2012. Geophysical and hydrological investigations at the west bank of Nile River (Luxor, Egypt). Environ Earth Sci. doi:10.1007/s12665-012-1525-2

Flathe M. 1955. Possibilities and limitations in applying geoelectrical methods to hydrogeological problems in the coaster area of Northwest Germany. Geophys Prosp. 3:95–110.

Ganerød GV, Rønning JS, Dalsegg E, Elvebakk H, Holmøy K, Nilsen B, Braathen A. 2006. Comparison of geophysical methods for subsurface mapping of faults and fracture zones in a section of the Viggja road tunnel, Norway. Bull Eng Geol Environ. 65(3):231–243.

Gheorghe A. 1978. Processing and synthesis of hydrological data. Junebridge Wells (Kent): Abacus Press. p. 122–136.

Hem JD. 1970. Study and interpretation off chemical characteristics of natural water. 2th ed. U.S. Geological Survey: Geologic survey water supply paper. p. 363–1473.

Ismail A 2003. Geophysical, hydrological, and archaeological investigation in the east bank area of Luxor, southern Egypt [PhD thesis]. USA: Department of Geology and Geophysics, University of Missouri-Rolla

Iyasele JU, David J, Idiata DJ. 2015. Investigation of the relationship between electrical conductivity and total dissolved solids for Mono-Valent, Di-Valent and trivalent metal compounds. Intl J Eng Res Rev. 3 (1):40–48.

Khalil MH. 2009. Hydrogeophysical assessment of Wadi El-Sheikh Aquifer, Saint Katherine, South Sinai, Egypt. J Environl Eng Geophys JEEG. 14(2):77–86.

Krasny J. 1993. Classification of transmissivity magnitude and variation. Groundwater. 31:230–236.

Maillet R. 1947. The fundamental equations of electrical prospecting geophysics. Geophysics 12(4):529–556.

Mayer XM, Ruprecht JK, Bari MA 2005. Stream salinity status and trends in south-west Western Australia. Western Australia: Department of Environment, Salinity and land use impacts series. Report No. SLUI 38.

Mohamed AME. 2003. Estimating earthquake ground motions at the Northwestern part of the Gulf of Suez [Egypt Ph.D. thesis]. Egypt: Ain Shams University. (Chapter 1)

Niwas S, Singhal DI. 1981. Estimation of Aquifer transmissivity from Dar – zarouk Parameters in Porus Media. J Hydrol. 50:393–399.

Oteri AU. 1981. Geoelectric investigation of Saline contamination of Chalk Aquifer by Mine drainage water at Tilmanstone, England. Geo-exploration. 19:179–192.

Sadek HS, Soliman SA, Abdulhadi HM; 1987: A correlation between the different models of resistivity sounding data to discover new fresh water fields in El Sadat City, Western Desert of Egypt. Proc. of the 7th International Mathematical Geophysics Seminar, Free University of Berlin, Berlin; 8–11 Feb. p. 329–346.

Sharaf El Dein MS, Essa KS, Youssef MAS, Karsli H, Diab ZE, Sayil N. 2019. Shallow geophysical techniques to investigate the groundwater table at the great pyramids of Giza, Egypt. Geosci Instrum Method Data Syst. 8:29–43. doi:10.5194/gi-8-29-2019

Singh KP, 2005. Nonlinear estimation of aquifer parameters from surficial resistivity measurements. Hydrol Earth Syst Sci Discuss. 2:917–923.

Velpen BPA. 1988. "RESIST", Version 1.0, A package for the processing of resistivity sounding data on pc compatibles [M. Sc. Research Project]. Deflt (the Netherlands): ITC.

Zohdy AAR, Bisdorf RJ. 1989. Programs for the automatic processing and interpretation of Schlumberger sounding curves in Quick Basic. U.S. Geol Surv Open File Rep. 89 (13):64.

Zohdy AAR, Eaton GP, Mabeym DR, 1974: Application of surface geophysics to groundwater investigations: in Tech. of water sources investigations of the U.S. Geol. survey book 2, chap, Dl. U.S. Dept. of the Interior, Geological Survey : U.S. Govt. Print.